Bollettino di Geofisica Teorica ed Applicata Vol. 56, n. 3, pp. 383-406; September 2015
DOI 10.4430/bgta0152

High frequency attenuation *k* parameter and Q_S 3D model for south-eastern Alps and north-western Dinarides

S. Gentili and G.F. Gentile

Istituto Nazionale di Oceanografia e di Geofisica Sperimentale – OGS, Udine, Italy

(Received: September 22, 2014; accepted: March 25, 2015)

ABSTRACT We estimated the spectral decay parameter *k* using waveforms produced by small-to-moderate earthquakes in the time period 1994-2011 in NE Italy and western Slovenia. We reconstructed the 3D distribution of the frequency independent part of the S waves' quality factor, Q_S, by using *k* values and S waves velocity V_S values as input. The Q_S model presented marked lateral and depth variations with a zone of low Q_S in the Kobarid area (western Slovenia). Considering these data together with available 3D distribution of V_P, V_P/V_S and shear modulus, we hypothesize that this is a highly fractured area permeated by fluids with variable pore pressure. At depths of 6-9 km, both in the central and in the western part of the area under study, two regions are characterized by significant lateral and in-depth Q_S contrasts. We interpreted these results in terms of amount of crack density and geological units.

Key words: body waves, seismic attenuation, seismic tomography, wave propagation, crustal structure, Europe.

1. Introduction

Friuli Venezia Giulia is one of the most seismic active regions of Italy, sited at the tip of the Adria plate in a convergent margin zone between Adria and Eurasia. The anticlockwise rotation of Adria causes a complex tectonic deformation. These characteristics make this region, together with western Slovenia, a natural laboratory for studies of seismic activity, strain field analysis and tomographic analysis. The Istituto Nazionale di Oceanografia e di Geofisica Sperimentale (OGS) seismic network was installed in 1977, in the area of the destructive 1976, M_L 6.4 Friuli earthquake, with the purpose of monitoring the area both for research activities and for emergency response by the civil protection authorities. The attenuation of seismic waves which propagate through the Earth can strongly influence the ground motion recorded at a site, thus modifying the energy content of the signal radiated from the source. Information on the attenuation in the area is important to obtain new insights on the crustal structure of the area with the purpose of contributing to seismic risk assessment.

The attenuation is modelled in literature either using the parameter *k* (e.g., Anderson and Hough, 1984), or using the quality factor *Q*, a dimensionless parameter introduced to quantify the fractional energy loss per cycle of oscillation as $Q = 2\pi E/\Delta E$ (Aki and Richards, 1980), where *E* is the energy and ΔE is the lost energy.

© 2015 – OGS

The attenuation due to high frequency spectral decay of acceleration amplitude Fourier spectrum has been modelled as (Cormier, 1982):

$$A(r,f) = A_0 e^{-\pi t^* f} \tag{1}$$

where A_0 depends on the source and the geometrical spreading and f is the frequency. In this model t^* is defined as:

$$t^* = \int_{path} \frac{1}{Q(r)V(r)} dr \tag{2}$$

where $Q(r)$ is the quality factor and $V(r)$ is the velocity of the waves.

Alternately, Anderson and Hough (1984) modelled high frequency acceleration spectrum, for frequencies greater than the corner frequency, as:

$$A(r,f) = A_0 e^{-\pi k f} \tag{3}$$

and Hough and Anderson (1988) modelled k as:

$$k = \int_{path} \frac{1}{Q_I(z)V(z)} dr \tag{4}$$

where Q_I is the frequency-independent part of Q, and Q is parameterized as:

$$Q(f)^{-1} = Q_D(f)^{-1} + Q_I{}^{-1} \cdot \tag{5}$$

Q_D and Q_I are respectively the frequency dependent and independent part of Q. In their work they use $Q_I(z)$ instead of $Q_I(r)$ as in their simplified model; Q_I depends only on the depth z (plane and parallel layers). However, their model can be generalized. Hough and Anderson (1988) noted that the model they used for k is the same of Cormier (1982) for t^* [see Eq. (1)], with the difference that only frequency independent part of Q is considered. In most literature on k estimation, the Q_D correction is performed before k estimation (Anderson and Hough, 1984; Castro *et al.*, 1997; Franceschina *et al.*, 2006; Bressan *et al.*, 2007). Vice versa, when t^* is estimated for attenuation tomography inversion, the frequency dependent term is usually neglected (Haberland and Rietbrock, 2001; Rietbrock, 2001; Olsen *et al.*, 2003; Eberhart-Phillips *et al.*, 2005). Estimates of Q dependence on frequency, based on the minimization of the variance of the spectrum misfit, give opposite results, depending on the analyzed area (Rietbrock, 2001; Stachnik *et al.*, 2004). Confusion arises also between the parametrization of Eq. (5) and (see e.g., Xie, 2010):

$$Q(f)^{-1} = Q_S(f)^{-1} + Q_i(f)^{-1} \tag{6}$$

where $Q_S(f)$ is the scattering Q caused by the random scattering process in the Earth media and $Q_i(f)$ is the intrinsic Q caused by Earth viscosity. Dainty (1981) assumes that Q_i is independent of frequency and that Q_S is proportional to frequency [and in this case Eqs. (5) and (6) coincide and $Q_i = Q_I$), but recent studies (Jackson, 2000; Jackson *et al.*, 2004) show a moderate dependence also of Q_i] on the frequency. Morozov (2008, 2010) proposes a model in which the dependence of Q on frequency is eliminated while the geometrical spreading can depend on frequency. Xie (2010) claims that Morozov (2008, 2010) model lacks a physical

basis and the fit of its model is just a curve fitting with first order Taylor series expansion of the one of Eq. (5). The reason for neglecting Q dependence on frequency in attenuation tomography studies is the difficulty in the evaluation of this term for the whole area under study and/or the lower dependence of the quality factor on frequency for higher frequencies. The latter reason is debated. For example, Adams and Abercrombie (1998), in a study on over 100 earthquakes recorded at the Cajon Pass borehole in southern California, showed a weak frequency dependence ($\sim f^{0.34}$) for frequencies above 10 Hz, while for frequencies below 10 Hz the dependence is stronger ($\sim f^{1.80}$). Raoof *et al.* (1999) in a study of southern California found a lower dependence ($\sim f^{0.45}$) for the frequency between 0.25 and 5.0 Hz.

Several different authors analysed the area under study in this paper and estimated the frequency dependence of Q for different frequency intervals (Console and Rovelli, 1981; Castro *et al.*, 1996; Govoni *et al.*, 1996; Malagnini *et al.*, 2002; Bianco *et al.*, 2005). In this paper, to describe the attenuation along each path, we considered the parameter k estimated from the seismograms. This choice differs from those of other authors, who parameterize the attenuation through the parameter t^*; for coherence with previous works on k estimate in the same area (Franceschina *et al.*, 2006; Gentili and Franceschina, 2011), we did not neglect the frequency dependence of Q. In particular, like Gentili and Franceschina (2011), we adopted Bianco *et al.* (2005) estimation, assuming constant regional frequency dependence $Q_D(f) = 251f^{0.7}$. We assumed also a negligible dependence of the geometrical spreading on frequency. Following the approach of Eberhart-Phillips *et al.* (2005), we estimated the difference between considering or not frequency dependence of Q in this area. In order to approximate the frequency dependent $Q_D(f)$ with a frequency independent term, we estimated its value at a frequency in the middle of the considered spectral window, i.e., in our case, 15 Hz. We found that considering frequency dependence does not affect too much the value of Q for high attenuation, while it is relevant for low attenuation. For example, for $Q_I = 20$ we have a very similar $Q = 19.8$ at 15 Hz. For very low attenuation, the effect of considering frequency dependence is larger: e.g., with $Q_I = 1000$ we have $Q = 626$ at 15 Hz. For coherence with previous papers notation, we called the frequency independent part of the quality factor for S waves simply Q_S instead of Q_{IS}.

This work should be regarded as a refinement respect to the simplified model of Gentili and Franceschina (2011), in which they found an approximately linear dependence of attenuation on distance valid for all the region, with anomalous higher attenuation in the western Slovenian area (Kobarid region).

The topic of this paper is a joint interpretation of the results of 3D Q_S inversion with the ones from tomographic inversion and the study of gravity anomalies (Bressan *et al.,* 1992, 2009, 2012; Gentile *et al.*, 2000).

2. Seismicity distribution, tectonics of the area and data set

The area we analysed is sited in NE Italy (Friuli Venezia Giulia region) and western Slovenia between the outer front of Southern Alps and the Periadriatic Lineament. It is included in a convergent margin zone between the Adria microplate and the Eurasian plate (see e.g., Castellarin *et al.*, 2006; Burrato *et al.*, 2008) and it is one of the most seismic active zones of Italy. The main tectonic features of the area are shown in Fig. 1.

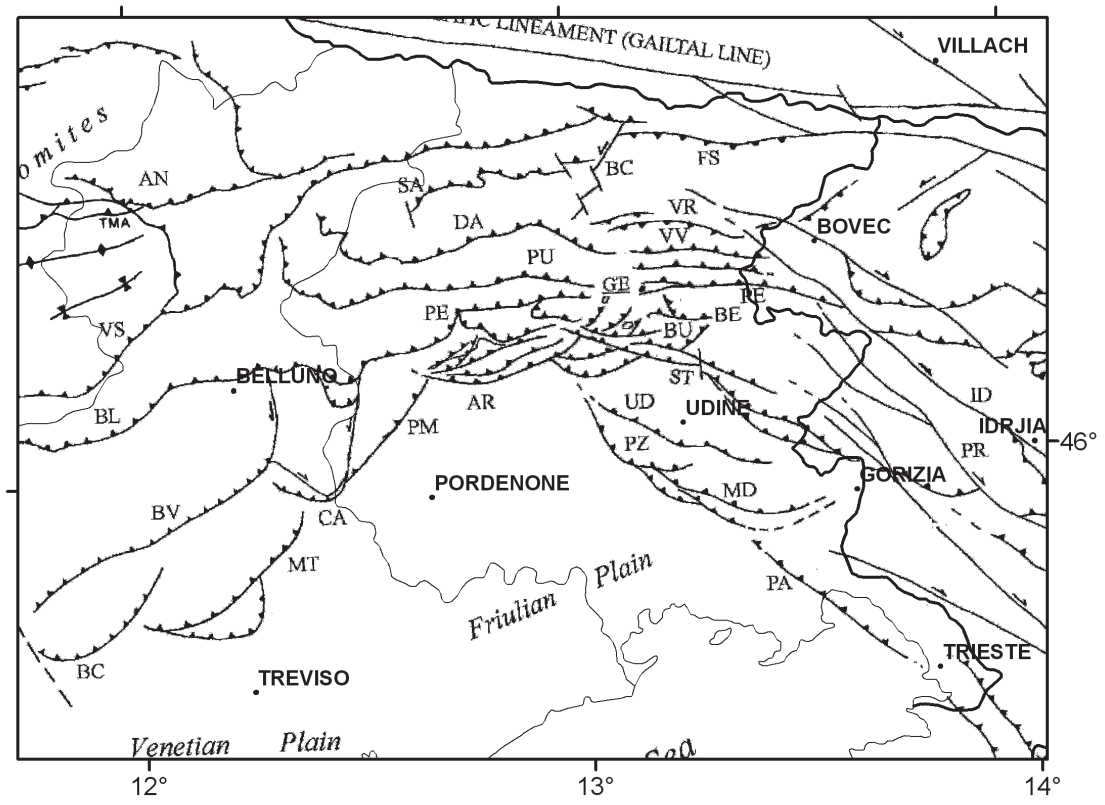

Fig. 1 - Simplified structural model of NE Italy and W Slovenia (modified from Carulli *et al*., 1990; Galadini *et al*., 2005; Castellarin *et al*., 2006). Legend (structures): ST, Stava-Collaccio fault; BC, Bassano-Cornuda fault; BV, Bassano-Valdobbiadene fault; BL, Belluno fault; VS, Valsugana fault; AN, Antelao fault; MT, Montello fault; CA, Cansiglio fault; PM, Polcenigo-Maniago fault; AR, Arba-Ragogna fault; PE, Periadriatic thrust; PU, Pinedo-Uccea fault; DA, Dof-Auda fault; SA, Sauris fault; BC, But-Chiarsò fault; FS, Fella-Sava fault; VR, Val Resia fault; ST, Susans-Tricesimo fault; UD, Udine-Buttrio fault; PZ, Pozzuolo fault; MD, Medea fault; PA, Palmanova fault; ID, Idrija fault; PR, Predjama fault.

The area is sited at the tip of the Adria plate. The progressive north-eastward pushing of the African plate, respect to the Eurasian plate, generates an anticlockwise rotation of the Adria microplate, which causes the present complex tectonic deformation (Mantovani *et al*., 1996). Several tectonic phases in the region inherited and reactivated the main pre-existing faults and fragmented the crust into different tectonic domains corresponding to different seismotectonic zones (Bressan *et al*., 2003). The eastern part of the region, in western Slovenia, is characterized by a strike-slip regime on the Dinaric faults. The Friuli area is characterized by thrust tectonics, mainly E-W oriented and south verging in the centre and NE-SW-oriented and SE-verging thrust in the western part (Bressan *et al*., 2003).

Fig. 2 shows both the historical and instrumental seismicity in the area. Brown squares correspond to earthquakes in CPTI04 catalogue (Gruppo di lavoro CPTI, 2004) from 1100 with intensity ≥ IX. In particular, 5 earthquakes are recorded: the January 25, 1348, Carnia earthquake (I_{MCS} = IX-X), the March 26, 1511, Slovenia earthquake (I_{MCS} = X), the 1695 February 25, Asolano earthquake (I_{MCS} = IX-X), the June 29, 1873, Bellunese earthquake (I_{MCS} = IX-X) and the October 18, 1936, Bosco del Cansiglio earthquake (I_{MCS} = IX). The other symbols

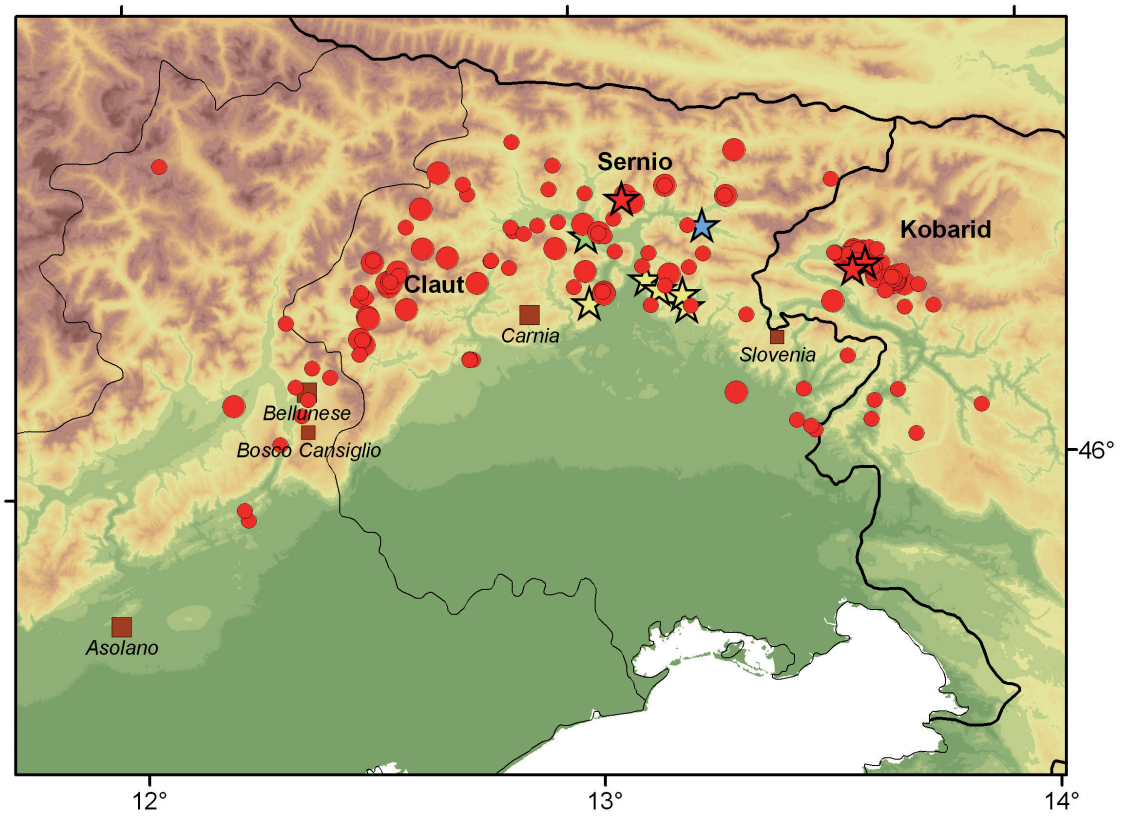

Fig. 2 - Seismicity in the area. Brown squares: historical seismicity (earthquakes with intensity ≥ IX are shown with squares dimensions proportional to earthquake intensity). Red symbols: seismicity with magnitude > 3.0 from 1994 to 2011. Stars: earthquakes with magnitude > 5.0. Yellow stars: 1976 swarm. Green star: 1977 Trasaghis earthquake. Blue star: 1979 Lusevera earthquake. Red stars: Kobarid and Sernio earthquakes.

correspond to instrumentally recorded seismicity. In particular, stars correspond to the events with magnitude ≥ 5.0 in the area. See the figure caption for more details.

Red symbols are the earthquakes used in this work. They are the 156 earthquakes with duration magnitude ≥ 3.0 recorded in the area from 1994 to 2011. In particular, there is a cluster of seismicity in correspondence with the two Kobarid 1998 and 2004 seismic sequences. Smaller clusters of lower magnitude seismicity were recorded also after the Sernio 2002 mainshock and in the Claut region [for seismic sequences in the area, see Gentili and Bressan (2008)]. The instrumentally recorded seismicity roughly follows the historical earthquakes distribution. The recording stations mainly belong to the Friuli and Veneto (FV) seismic network, managed by OGS. Such data have also been integrated with data obtained by the Slovenian seismic network (during the Kobarid 2004 seismic sequence - 3 stations) and temporary network [both OGS in the Claut area from 2005 March to 2008 February (4 stations) and Slovenia in the Kobarid area during the 2004 seismic sequence (2 stations)]. All earthquakes have been re-located by a 3D crustal model using SIMULPS12 (Evans *et al.*, 1994) tomography code (Bressan *et al.*, 2009; Bressan, private communication, 2012) obtaining high accuracy hypocentres locations. In particular, the horizontal and vertical location errors do not exceed 0.05 and 0.10 km, respectively (Bressan *et al.*, 2009).

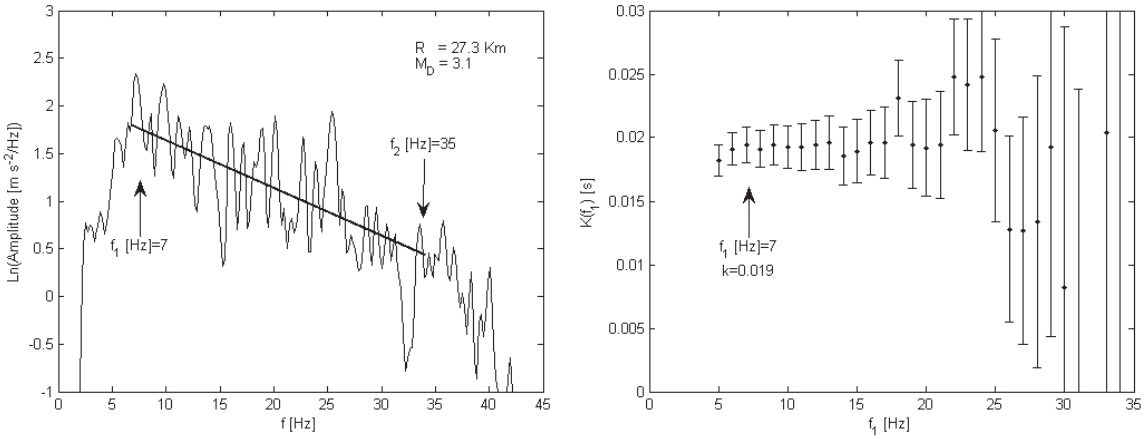

Fig. 3 - An example of spectral decay parameter estimation. Left panel: acceleration spectra and linear regressions used to obtain the single record estimate of the k parameter; right panel: k estimates and corresponding standard deviations as function of the lower limit of the frequency bandwidth adopted for the linear regression, f_1. The best estimate of k and the corresponding value of f_1 are indicated by an arrow.

3. Method

We estimated the k parameter for S waves. Assuming a negligible dependence of the geometrical spreading on frequency, we estimated the parameter from the slope of the amplitude Fourier spectrum of acceleration data after correction for the frequency dependent part of the quality factor (see e.g., Franceschina *et al.*, 2006). Both the N-S and the E-W horizontal components of the signal were used. The S wave window was manually selected for both traces and the resulting data were tapered by 5% cosine taper and padded with zeros before applying the FFT. The resulting spectra were smoothed by a sliding Hann window (Oppenheim and Schafer, 1999) of 0.5 Hz half-width. The spectral band adopted for the analysis was determined by selecting the part of the spectrum (a frequency band $[f_1, f_2]$ with $f_1 > 5$ Hz) where a linear decay was clearly evident. We adopted a threshold on the duration magnitude of analysed earthquakes of $M_D > 3.0$ in order to ensure the validity of the condition $f_1 > f_C$, where f_C is the corner frequency, and therefore the Anderson and Hough (1984) fist order approximation of spectrum shape (see Fig. 3). In fact, accordingly with previous analysis in this area (Bressan *et al.*, 2007) for $M_D = 3.0$ $f_C \cong 4.6$ Hz. We selected f_2 as the frequency at which the noise level starts contaminating the signal that, in this study, ranged from 20 to 45 Hz. In order to determine f_1, accordingly with Gentili and Franceschina (2011), we estimated k values for increasing values of the minimum frequency; we plotted the obtained k as function of f_1 and selected $k(f_1)$ values in an observed range of stability of this function by a visual inspection of each plot; f_1, generally depending on event size, ranged from 5 to 10 Hz. Fig. 3 shows an example of spectral decay parameter estimation.

In order to fit the amplitude spectrum, we used the L1 norm solution method. This method minimizes the absolute difference of the residuals rather than the squared differences, thus decreasing the influence of outliers on results. The k values estimated from the two horizontal components of each record were averaged by computing the corresponding weighted mean and

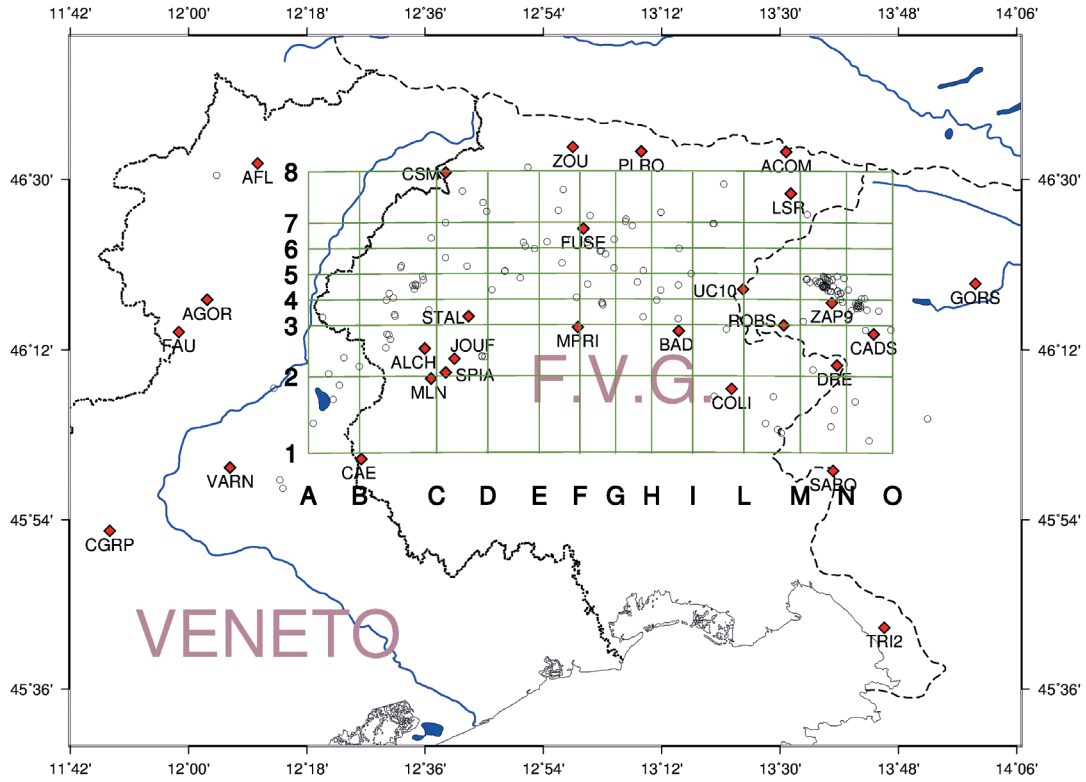

Fig. 4 - Grid of the 3D Q_S tomographic inversion. Diamonds: location of seismic stations used for the inversion. Circles: earthquakes used for Q_S inversion.

standard deviation. In order to increase the robustness of the method, the weights were chosen as the inverse of the error of each single fit.

In attenuation tomography the equation to be solved is:

$$y=\mathbf{M}x+e \qquad (7)$$

where y is the vector of the differences between the real values of k and those obtained with the theoretical model, **M** is the matrix of the partial derivatives respect to **QV**, **QV** is the element wise multiplication of the **Q** quality factor 3D matrix and the **V** velocity 3D matrix, x is the variation of **QV** along the path (model parameters) and e is the vector of errors, which can be random, such as the uncertainty in k estimation, or non-random, such as errors caused by inadequate parameterization. It is important to remark that in Q inversion procedure the S waves velocity field is taken as input. It is, therefore, necessary to use a reliable velocity information in order not to bias results on Q inversion.

To invert the k data we used the same grid used by Bressan *et al*. (2012) in 3D tomographic inversion of velocity in the area (see Fig. 4). The grid extends 114 km in E-W direction and 55 km in N-S direction. The grid centre has latitude 46.33° N and longitude and 13.08° E. The W-E grid nodes are at X: -60, -50, -35, -25, -15, -7, 0, 7, 15, 25, 36, 45, 54 km; the S-N grid nodes are at Y: -35, -20, -10, -5, 0, 5, 10, 20 km; the Z nodes are at depth 0, 2, 4, 6, 8, 10, 12, 15, 22 km with a layer at negative 3 km depth to account for the Earth's topography. The X-axis is positive to the east, the Y-axis is positive to the north. The velocity of S waves in the medium is parameterized by assigning velocity values obtained in the Bressan *et al*. (2012)

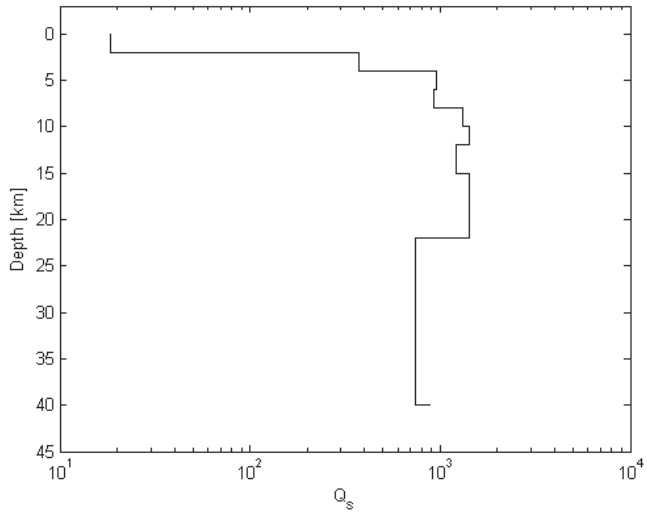

Fig. 5 - 1D Q_S starting model obtained by a genetic algorithm technique.

paper at the nodes of the grid. Bressan *et al*. (2012), used 394 events from 1988 to 2004 with duration magnitude between 1.4 and 5.1 and performed an iterative simultaneous inversion of hypocentral parameters and 3D velocity structure with a damped least squares technique using SIMULPS12 (Evans *et al*., 1994). We used 977 3D seismic traces corresponding to 156 events from 1994 to 2011 recorded by 28 seismic stations with duration magnitude between 3.0 and 5.7. The lower number of earthquakes is due to our considered magnitude range.

In every tomographic linearizing procedure, due to the non-uniqueness of the solution, a starting realistic crustal model is essential for avoiding error and biases in the results. In the Friuli area no previous knowledge for a valuation of the Q_S field is available; so a heuristic search was employed to find the 1D starting crustal model, which does not use linearization method. We adopted a genetic algorithm technique (Goldberg, 1989). In our case the individuals are the average Q_S values for each layer and the environmental law is defined by the total weighted RMS value obtained by a tomographic 1D inversion. The number of the generations and of the individuals grows exponentially with the number of the parameters. We had eleven crustal layers that were the parameters to invert. For such a number of parameters, in order to avoid too numerous populations and too many generations, a micro genetic technique was applied. The David L. Carroll GAFORTRAN code (Carroll, 2001) with a micropopulation of five individuals was utilized, using as cost function SIMUL2000 code (the last version of SIMULPS12) minimizing the total weighted RMS; 600 generations were generated. The starting fitness (RMS) of the best individual was 0.0243 and the average fitness of the first population was 0.0244, the cost-function stabilizes over a value of 0.0148 with an average value of 0.0152 after the 318th generation. The final Q_S values are shown in Fig. 5.

Due to unavailability of experimental data in the region analysed, these results can be compared with the ones of studied regions. The very low value of Q_S between 0 and 2 km (Q_S = 18.5), corresponding to a high attenuation of the medium, is compatible with experimental attenuation measures from borehole recording made by Abercrombie (1998) in California. The rapid increase of Q_S value with depth is similar to Californian results [see Hauksson and Shearer

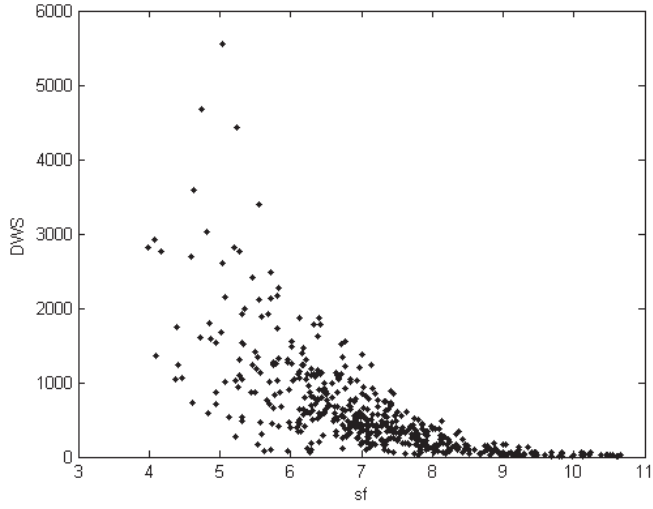

Fig. 6 - Derivatives Weight Sum (DWS) as function of Spread Function (sf).

(2006) model], even if the values of the parameter for larger depths are smaller of a factor 2 in California (approximately 700 instead of 1400). These differences may be connected with the different tectonic settings or with the fact that Hauksson and Shearer (2006) do not consider the frequency dependent part of Q_S.

Starting from the previous 1D Q_S Earth model, we performed the 3D inversion using the program SIMUL2000 (Eberhart-Phillips, 1993; Thurber, 1993; Thurber and Eberhart-Phillips, 1999). The code applies an iterative damped least squares method. In the inversion, as suggested in SIMUL2000 code, the earthquakes hypocentres and origin times were kept fixed. The Q_S crustal values are inverted using a damping value chosen evaluating the trade-off curve of the data variance versus model variance achieved after single iterations (Eberhart-Phillips, 1986, 1993). In our case, we chose a damping value of 0.002 corresponding to a data variance of 4433 and a model variance of 2.18×10^{-4}. After 4 iterations the program terminated for F-test with a weighted RMS of 0.0115 against the starting one of 0.0148.

4. Resolution and reliability of the results

An estimate of the reliability of the data is vital for the interpretation of seismic tomographic images. In fact, a bad distribution of stations and earthquakes causes inhomogeneity in the accuracy of results. We approached this problem by using the model resolution matrix. Each row of the resolution matrix is the averaging vector for a single parameter (see e.g., Toomey and Foulger, 1989). It describes the dependence of the value of an estimated parameter on the values of all the other parameters. Toomey and Foulger (1989) show two examples of plot depicting the elements of the averaging vector in the three-dimensional space of the studied volume. Qualitatively, a good resolution for a grid node value (parameter) is obtained when its averaging vector is non-zero only in the vicinity of the node (compact averaging vector). However, the plot of each grid node is impractical when the grid contains hundreds of nodes. An average relative

measure of the density of seismic rays near a node is given by the Derivatives Weight Sum (DWS). In a non-uniform and then not evenly illuminated field, a single node much more resolved than its neighbors can lead to a smearing effect: its value conditions the values of the adjacent nodes. In order to account for this effect, Michelini and McEvilly (1991) introduced the spread function of a node of the grid. The well-sampled nodes, characterized by high DWS, generally correspond to low level of spread function. There is scatter on the trend because the averaging vector depends on the geometry of the rays in its surrounding and not just on the density of rays. For this reason, estimates of the resolution, based on DWS only, supply only qualitative results (Toomey and Foulger, 1989). Like in Toomey and Foulger (1989), we examined a test set of averaging vectors and we estimated a threshold value of 7 for the spread function under which we consider the resolution acceptable. Fig. 6 shows the DWS values versus spread function values.

Fig. 7 shows the distribution of the spread function S on the grid in horizontal layers. The layers at 4, 6 and 8 km deep, characterized by wide central zones with S less or equal 7, are the most reliable ones. Shallower and deeper layers are unevenly illuminated by the seismic ray paths; there are only smaller areas where the smearing effect is not prevalent: at 0 and 2 km only the southernmost zone and below 8 km the westernmost one.

Another estimate of the tomography results is based on the capability to reconstruct the Q field on synthetic data characterized by the same distribution of earthquakes and recording stations. The checkerboard test consists in alternating adjacent nodes of two different Q_S values Q_1 and Q_2, where $Q_1=Q_m+a$ and $Q_2=Q_m-a$, Q_m is the mean Q_S value and a is a parameter. The synthetic k are estimated keeping the hypocentres fixed. The test consists in evaluating the capability to reconstruct the original field starting from a uniform Q_m field. We performed the checkerboard test with Q_m = 200 and a = 80, obtaining in such a way a checkerboard with variations of ±40% (see Fig. 8a for an example of input data for one layer). We repeated the test adding to synthetic k a random Gaussian noise with sigma equal to 2.5% of the data value, compatible with the errors in k value estimation. Fig. 8b shows the checkerboard test results without noise added, superimposed an isoline of the S value of 7. In the layers deeper than 2 km, the checkerboard test conformity with the 7 spread function isoline seems to be clear. Adding noise does not significantly worsen the Q_S values field restitution (Fig. 8c).

The last test was performed following the approach of Shurr *et al*. (2003) and De Siena *et al*. (2010): a synthetic test with anomalies comparable in size and amplitude with those observed in real data, but different geometry has been endowed to check the output size and intensity of anomalies. This test allows to explore the true resolving capability in zones of maximum interest. We simulated a model with parallel flat layers with the same values of Q_S of the output of the genetic algorithm, on which we superimposed two high Q_S anomalies in the western and central part, overlapping a low Q_S anomaly, and a larger low Q_S anomaly in the eastern part (see Fig. 9a). We added to the simulated k values the same error in the data used for the checkerboard test. This last test shows that the anomalies are generally well resolved (see Fig. 9b), although, like in Schurr *et al*. (2003), amplitudes may be underestimated due to the damping; in particular the best resolved region is the one in the eastern part, due to the large illumination of the area.

It is important to remark that the results below 12 km are affected by the the limitation of the distribution of earthquakes and stations for both Q_S and input V_S data [see Eq. (4)]. For this reason, we took into account the results on the inversion only for depth shallower than 12 km.

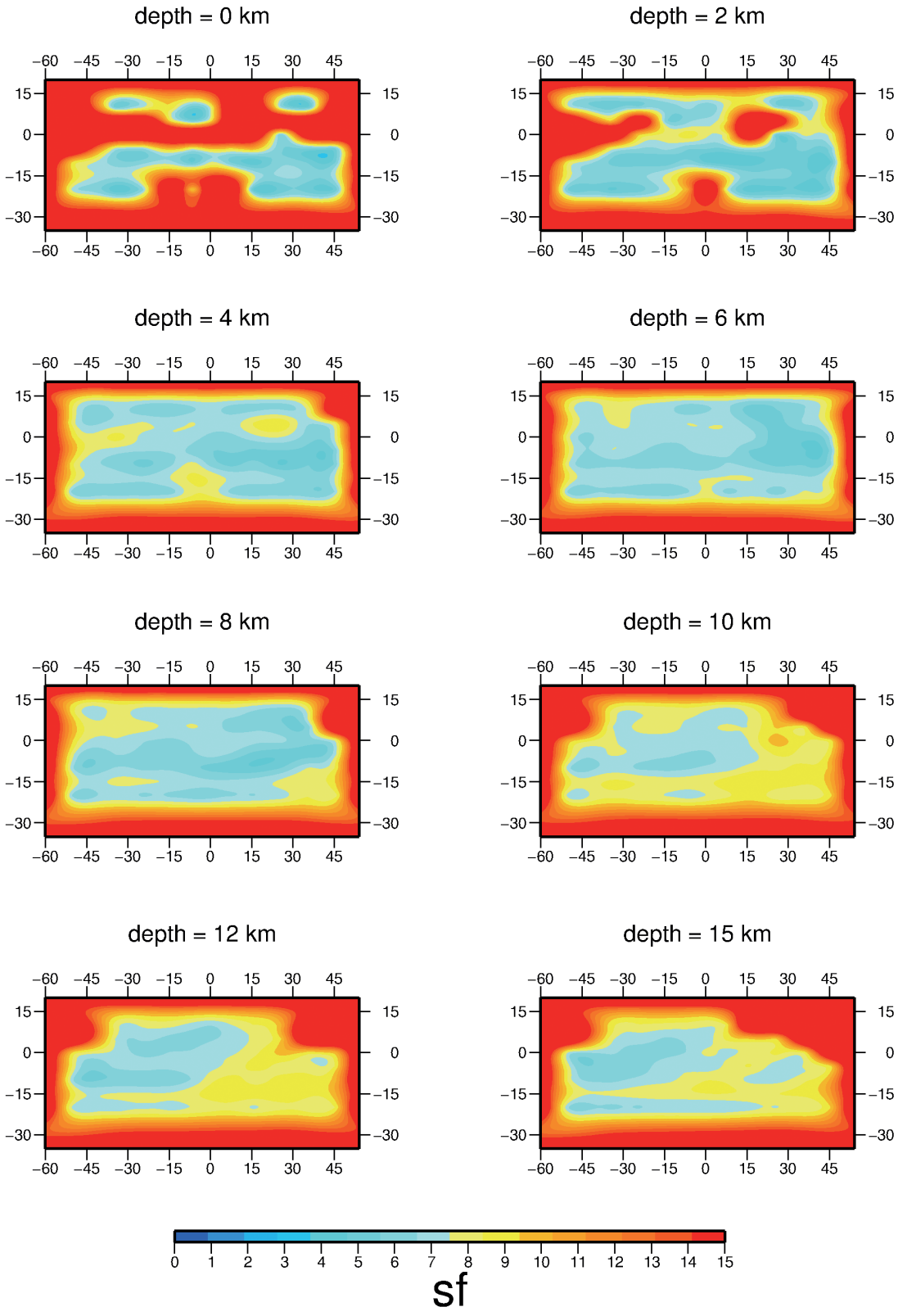

Fig. 7 - Spread Function (sf) describing resolution of the 3D Q_S inversion at 8 slices (0, 2, 4, 6, 8, 10, 12, 15 km).

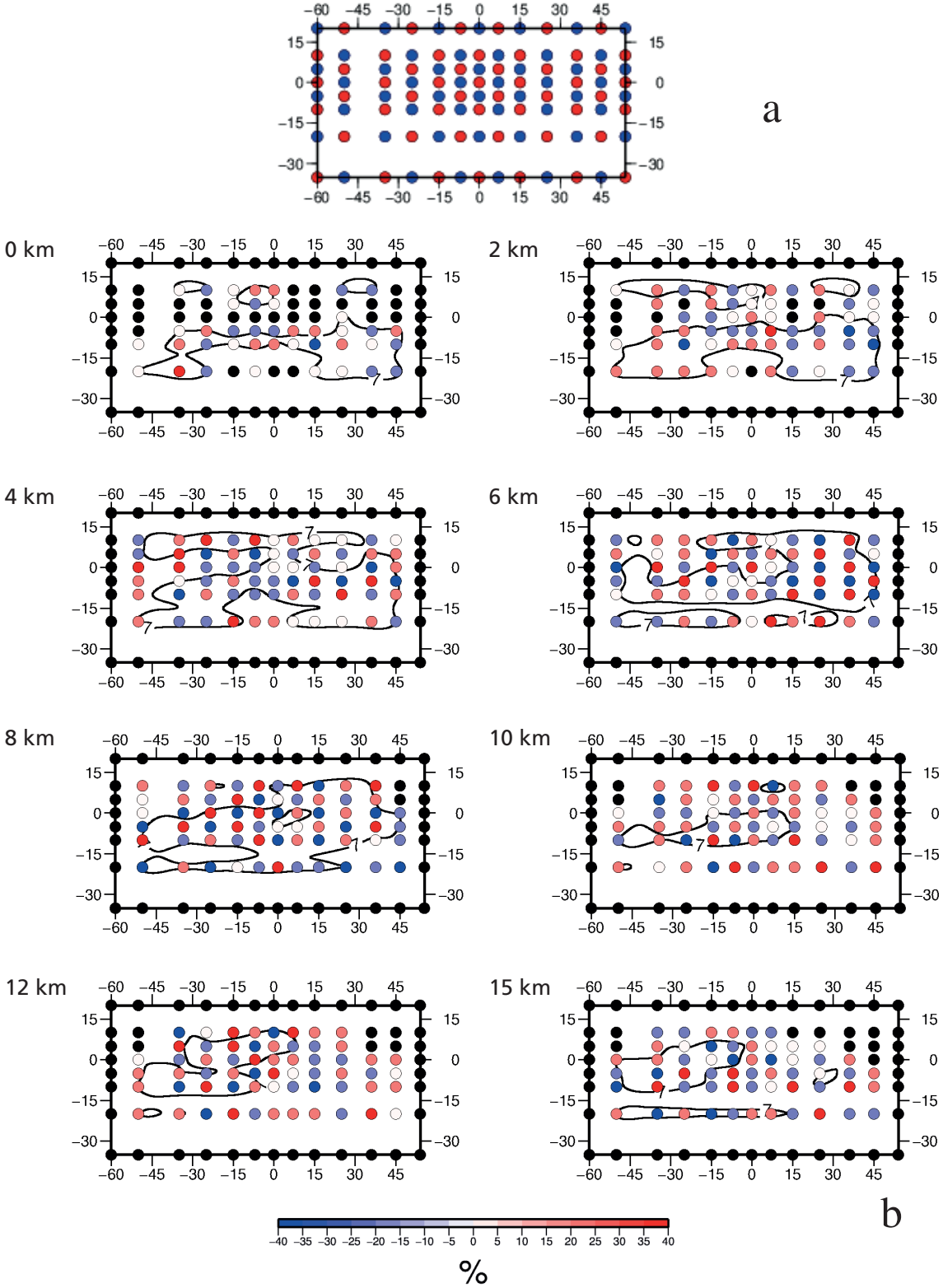

Fig. 8 - Checkerboard test of the 3D Q_S inversion at 8 slices (0, 2, 4, 6, 8, 10, 12, 15 km): a) an example of input layer; blue: -40%, red: +40%; b) checkerboard test results without noise c) with 2.5% noise added to the data. Color corresponds to the percentage difference respect to the mean value.

c

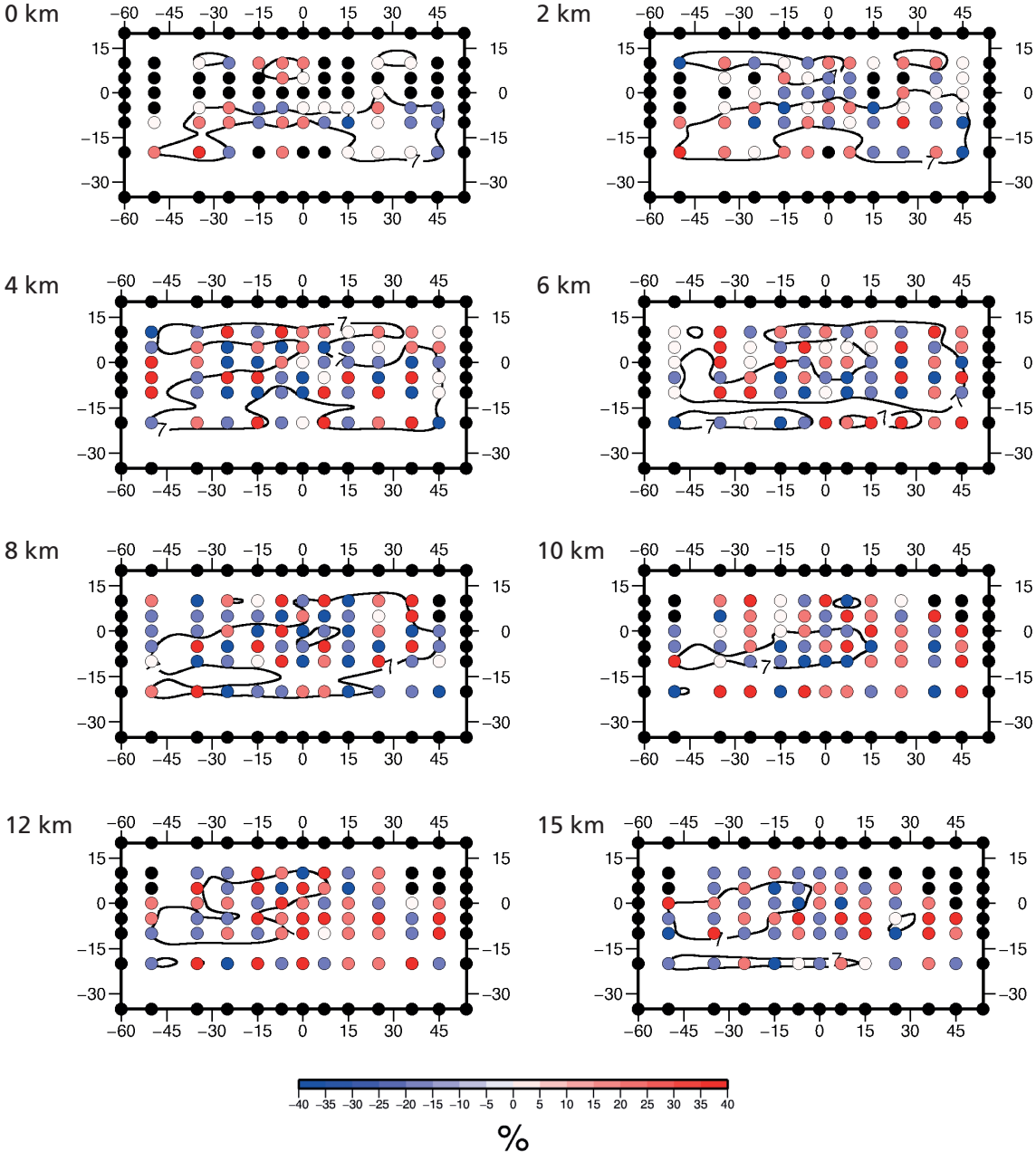

Fig. 8 - continued.

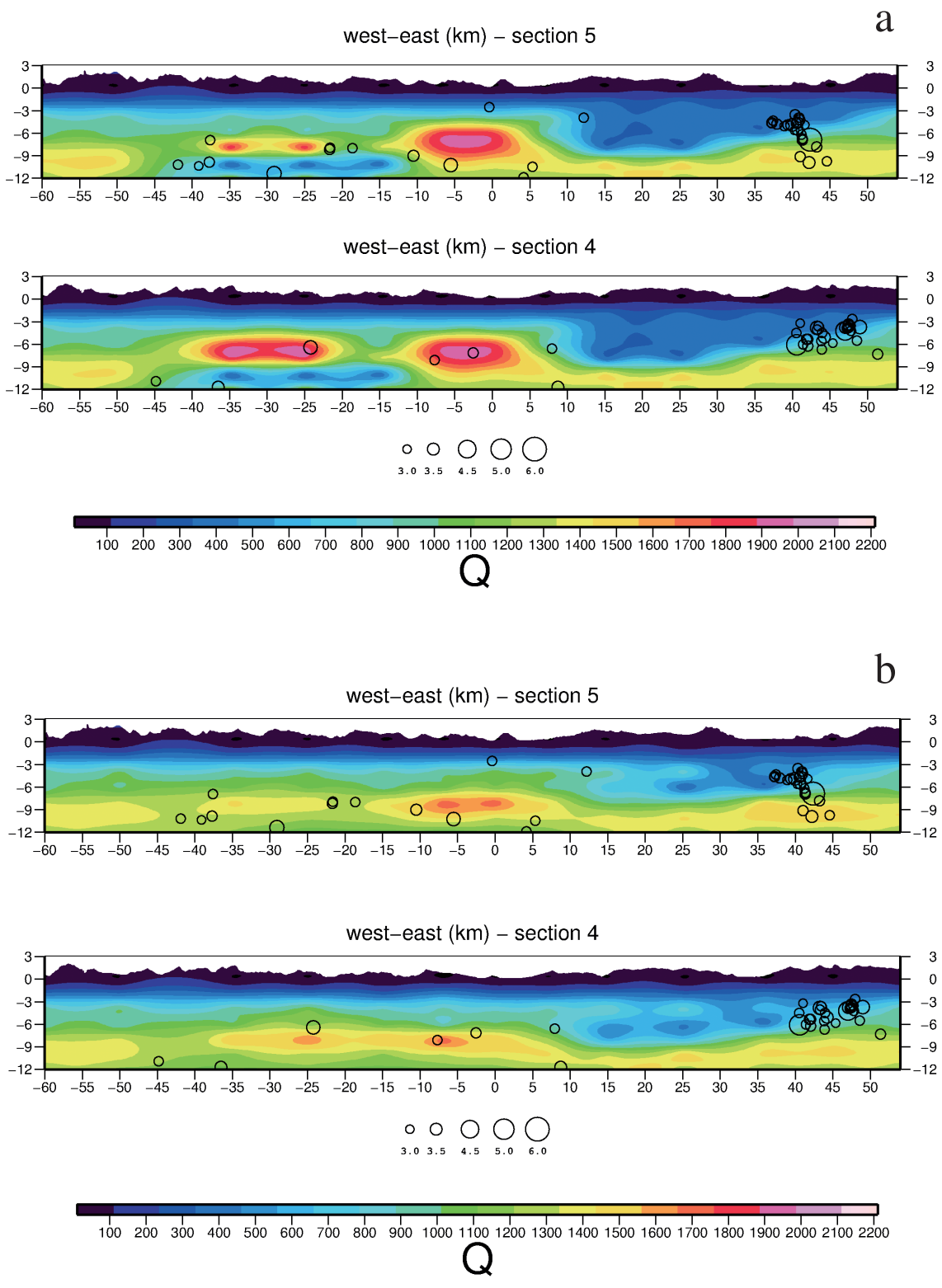

Fig. 9 - Q_S synthetic anomaly test: a) input synthetic model; b) recovered model for sections in (a) after adding a random Gaussian noise with sigma equal to 2.5% of the data value.

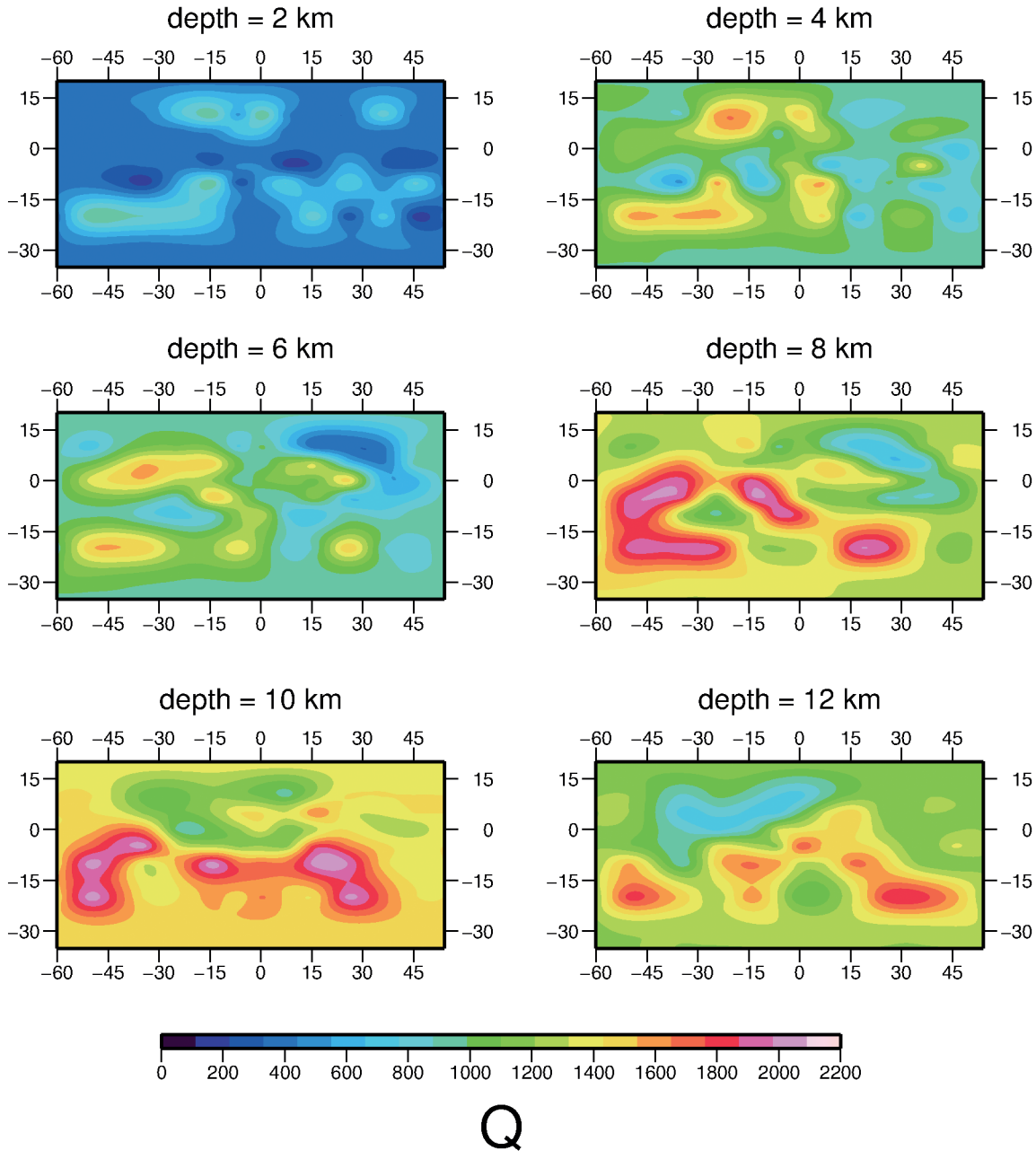

Fig. 10 - Tomographic images of Q_S at depth slices 2, 4, 6, 8, 10, 12 km.

5. Results

Fig. 10 shows Q_S images at 6 depth slices. The vertical sections 4 and 5 of the tomographic 3D reconstruction of Q_S are shown in Fig. 11; the earthquakes are indicated as circles whose size corresponds to the magnitude. For the generic n^{th} section with coordinate y_n, earthquakes in the range $[(y_{n-1}+y_n)/2, (y_n+y_{n+1})/2]$ are projected.

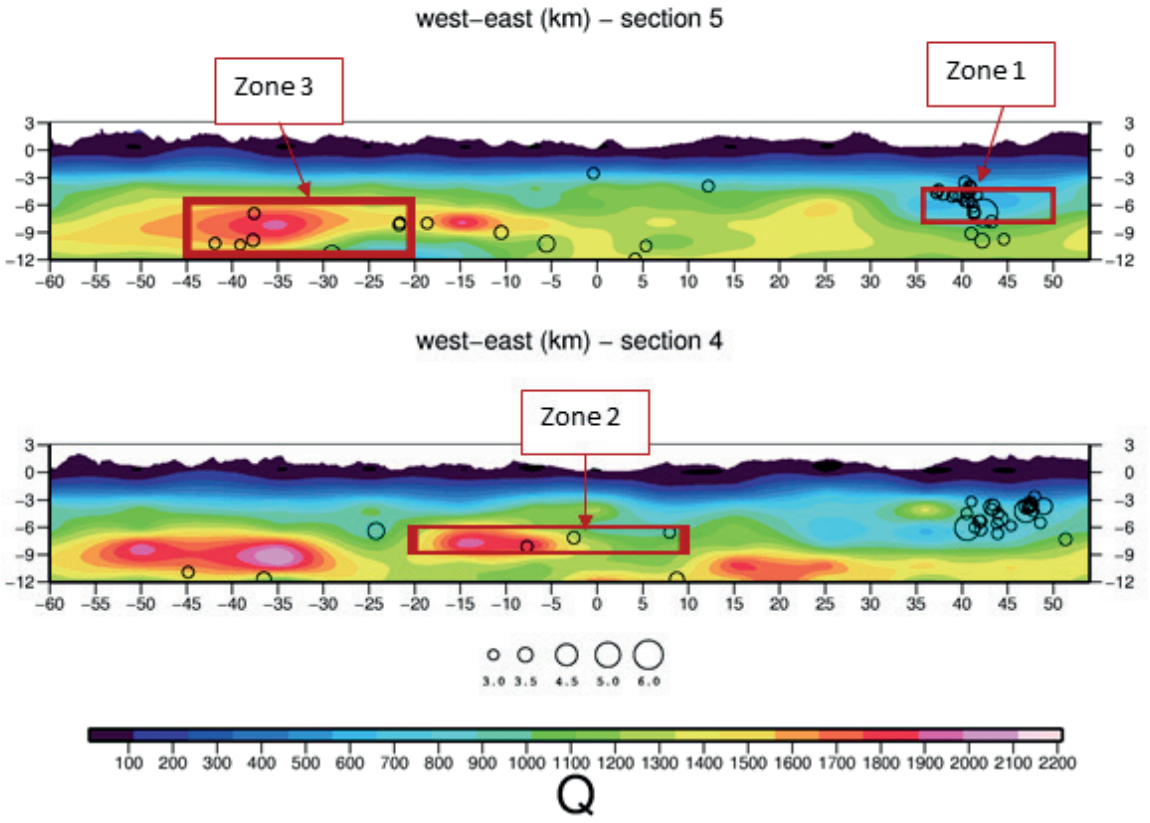

Fig. 11 - Vertical cross-sections 4 and 5 (see Fig. 4) of the 3D tomographic Q_S image. Circles represent earthquakes. Circle size is proportional to earthquakes magnitude.

The Q_S images are characterized by marked lateral and depth variations. At large scale, three zones can be recognized with different attenuation pattern related to the geologic-structural heterogeneity of the upper crust. The structural heterogeneity associated with the variations of the mechanical properties of rocks has been highlighted by the Sequential Integrated Inversion (SII) of tomographic images and gravity data of Bressan *et al.* (2012) applied to the same study area, which provided the 3-D V_P, V_P/V_S and elastic moduli pattern.

Large attenuation, resulted from low Q_S values, is observed in the rightmost part of the studied area (Fig. 11, zone 1), corresponding to the Kobarid region (western Slovenia), in good agreement with the results of Gentili and Franceschina (2011). Fig. 12 shows an example of the anomalous attenuation in Kobarid on the k attenuation parameter: earthquakes from the Kobarid region (white circles) exhibit higher values of k (higher attenuation) respect to the general regional trend of k with distance (grey circles). Low values of Q_S have been associated with the presence of cracks, to high pore fluid pressures and to low heat flow (Hauksson and Shearer, 2006; Zhou *et al.*, 2011). We emphasize that the area investigated in the present paper is characterized by relatively low values of heat flow: 50-60 mWm^{-2} (Cataldi *et al.*, 1995) in the Friuli region (north-eastern Italy) and 30-40 mWm^{-2} (Lapanje *et al.*, 2011) in the Kobarid region (western Slovenia). The results of Bressan *et al.* (2012) confirm the former tomographic V_P and V_P/V_S models, obtained by Bressan *et al.* (2009) in the Kobarid region on a finer grid. The tomographic images showed a large variability of the V_P and V_P/V_S pattern with marked

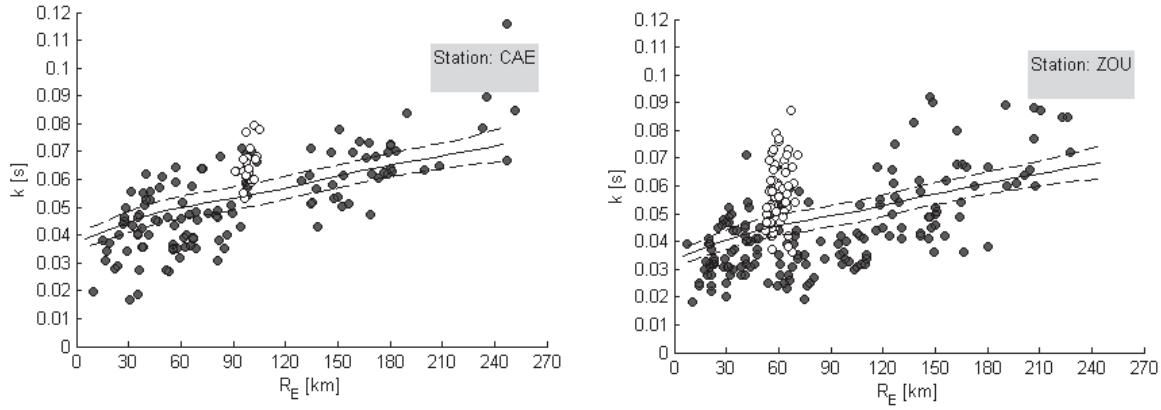

Fig. 12 - Functions $k(R_E)$, where R_E is the epicentral distance, with the corresponding 95% confidence limits (solid and dashed lines, respectively), estimated for 2 stations of the network with a non-parametric approach. Circles represent the single-record estimates of the k parameter. Open circles correspond to the k estimates obtained with Kobarid region earthquakes.

lateral and depth variations in the Kobarid zone, related to lithological inhomogeneity and to the different amount of cracking and fluid pressure. The 3-D SII tomographic model evidences a high rigidity body in comparison with the surroundings, placed at depth between 4 and 7 km (see Figs. 13, 14 and 15). The high rigidity structure is characterized by P-wave velocity range 6.2-6.8 km/s, by V_P/V_S values varying from 1.74 to 1.86 and shear modulus ≥ 3.2×10^{10} Nm^{-2}. It was associated (Bressan *et al*., 2009) with a rock mass of prevailing platform limestones and dolomitic limestones of Mesozoic age (see Fig. 16). The variability of V_P/V_S values was attributed to the different amount of fracturing and hence to the brittleness. The upper layers are characterized by lower P-wave velocities (4.8-6.2 km/s), by V_P/V_S values in the range 1.71-1.88 and shear modulus varying from 1.8 to 2.5×10^{10} Nm^{-2}. These values were associated with chert limestones, sandstones and marls of Mesozoic-Cenozoic age. Low V_P/V_S values associated with seismicity were explained by Powell *et al*. (2006) as highly fractured and fluid saturated rocks with high pore pressure, while they are attributed by Mjelde *et al*. (2003) to sedimentary rocks with sand/shale relatively high. Furthermore, the large variability and the heterogeneous pattern of V_P/V_S values reflects the heterogeneous crustal structure of the area, dominated by the extended strike-slip Ravne fault (Kastelic *et al*., 2008), characterized by branching and minor splay faults.

In short, the joined interpretation of Q_S and the tomographic data of Bressan *et al*. (2012) suggests that the low values of Q_S in the Kobarid area are caused by large amount of fracturing and variable pore pressure of the fluids, as suggested by the heterogeneous V_P/V_S pattern.

The Q_S regions are characterized by significant lateral variation in the central part of the area at 6-9 km depth (Fig. 11, section 4, zone 2). The high Q_S structure is associated with V_P values varying from 6.3 to 7.0 km/s, range V_P/V_S values 1.72-1.90, shear modulus values between 3.1 and 4.0×10^{10} Nm^{-2}. Low Q_S regions are characterized by V_P values 6.0-7.0 km/s, V_P/V_S values 1.81-1.98, shear modulus values $2.6\text{-}3.9\times10^{10}$ Nm^{-2} (Bressan *et al*., 2012). The high Q_S regions correspond to a geologic unit mainly composed of Triassic and dolomitic limestones, while the low Q_S ones are related to alternation of limestones from mixed carbonate-clastic platform, dolomitic limestones and chert limestones of Triassic-Jurassic age. The variation in

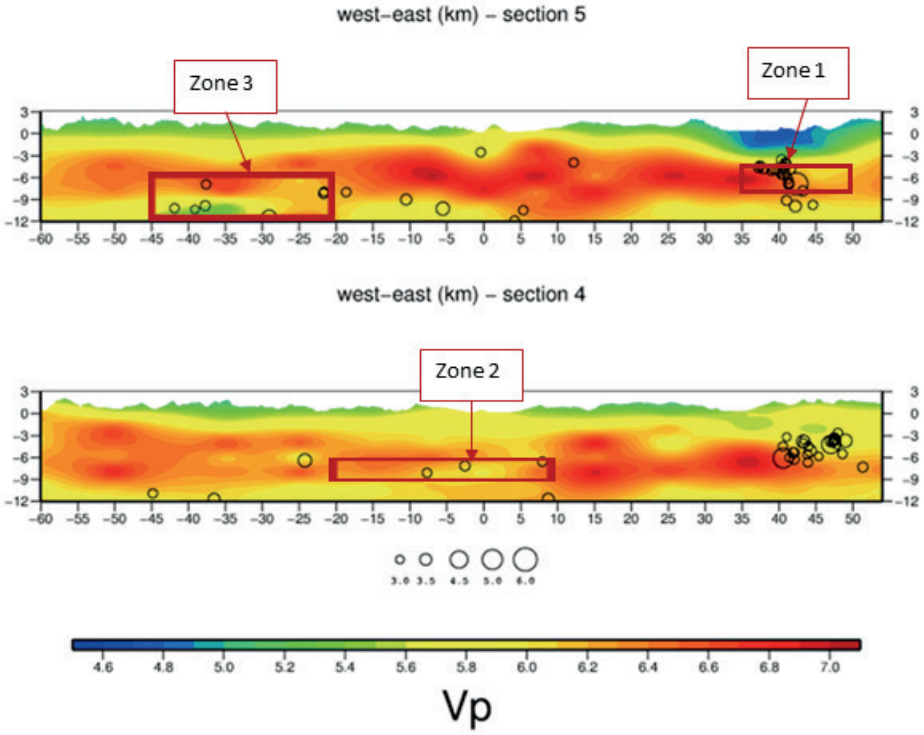

Fig. 13 - Vertical cross-sections 4 and 5 (see Fig. 4) of the 3D tomographic V_P image from Bressan *et al*. (2012) results. Circles represent earthquakes used in our paper. Circle size is proportional to earthquakes magnitude.

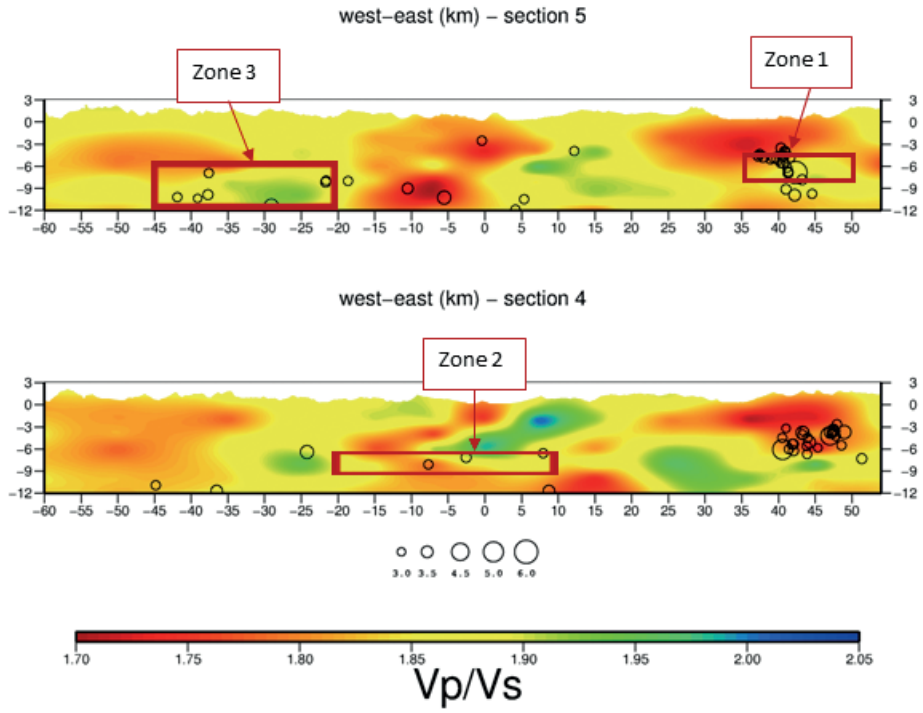

Fig. 14 - Vertical cross-sections 4 and 5 (see Fig. 4) of the 3D tomographic V_P/V_S image from Bressan *et al*. (2012) results. Circles represent earthquakes used in our paper. Circle size is proportional to earthquakes magnitude.

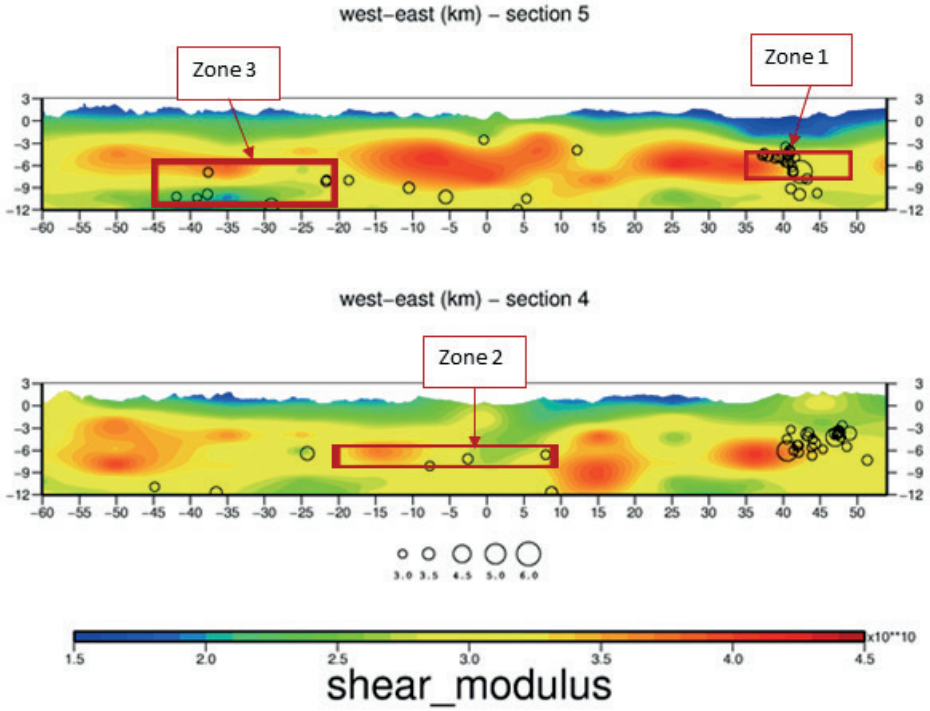

Fig. 15 - Vertical cross-sections 4 and 5 (see Fig. 4) of the 3D shear modulus image from Bressan *et al*. (2012) results. Circles represent earthquakes used in our paper. Circle size is proportional to earthquakes magnitude.

the mechanical properties of the geologic units seems to play a role even in this case. However, the low Q_S structure is generally characterized by V_P/V_S values higher than the high Q_S structure, suggesting higher crack density.

The Q_S images highlight a heterogeneous lateral and deep pattern of the attenuation in the western side of the study area (Fig. 11, section 5, zone 3). A zone of high Q_S values (low attenuation) is recognized at 6-8 km depth, overlapping a zone of low Q_S values (high attenuation). The high Q_S structure is characterized by P-wave velocity range 6.2-6.8 km/s, V_P/V_S values 1.78-1.90 and shear modulus varying from 2.9 to 3.9×10^{10} Nm^{-2} (Bressan *et al.*, 2012). The geologic structure is mainly made-up of dolomitic limestones of lower Triassic age with variable density of cracks. The low Q_S zone is characterized by the V_P range 5.7-6.4 km/s, V_P/V_S values 1.85-1.95 and a relatively low shear modulus, ranging between 2.0 and 2.9×10^{10} Nm^{-2}. These values are associated with the following stratigraphic-geologic sequence: limestones originated from mixed carbonate-clastic platform of Triassic age and from sandstones and limestones of Palaeozoic era. The variation in attenuation can be assigned mainly to the variation of the mechanical properties of the geologic units. The rocks, pertaining to the high Q_S zone, are characterized by more hardness and rigidity.

By summarizing, the Q_S anomalies appear related to the mechanical heterogeneity of the crust, the different geologic units and the different amount of crack density. The variation in the V_P/V_S pattern (Bressan *et al.*, 2012) can be presumably driven also by variable pore pressure, but there are not reliable and exhaustive data about crustal fluids in this area.

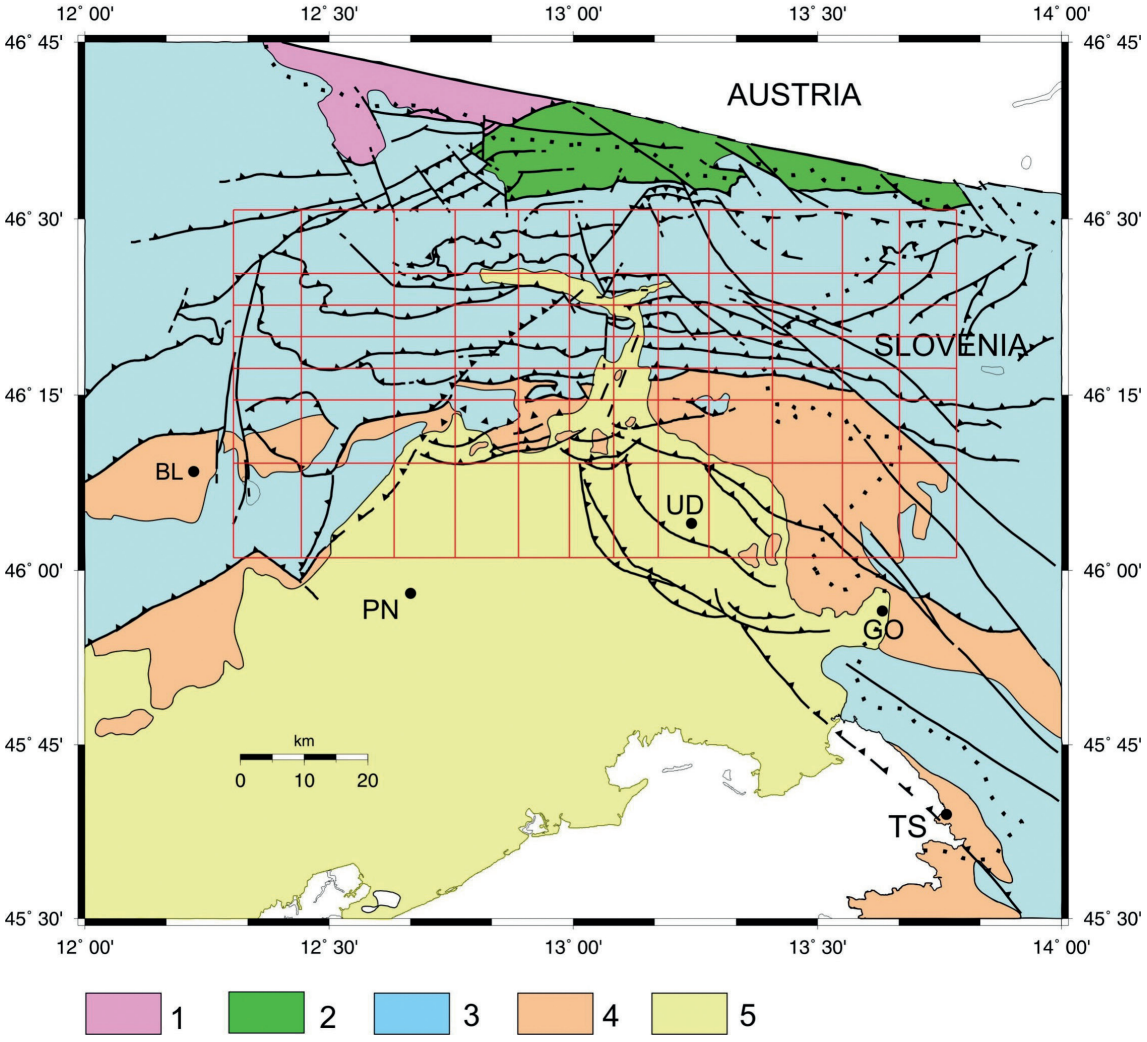

Fig. 16 - Schematic geological map (from Bressan *et al.*, 2012). The grid of the tomographic Q_S inversion is also plotted. Symbols: 1) Hercynian very-low metamorphic basement (Ordovician-Carboniferous); 2) Paleocarnic Chain, non- and anchimetamorphic succession (Upper Ordovician-Carboniferous): sandstones, limestones and locally volcanic deposits; 3) Upper Carboniferous and Permo-Mesozoic carbonate successions: dolomitic limestones, carbonate-clastic platform limestones, chert limestones and locally sandstones, marls; 4) Flysch (Upper Maastrichtian-Middle Eocene) and molassic sequence (Miocene); 5) Quaternary covers. Solid and dashed lines: subvertical faults; barbed lines: thrusts. Towns: BL, Belluno; PN, Pordenone; UD, Udine; GO, Gorizia; TS, Trieste (from Bressan *et al.*, 2012).

We emphasize that the investigated area is characterized by a polyphase deformational zone, resulting from the superposition of several Cenozoic era tectonic phases (Venturini, 1991), with different orientation of the principal axes of stress. Each tectonic phase inherited and re-activated the geological deformations of the previous phase producing a complex deformation pattern and different tectonic domains. The upper crust is characterized by marked lateral and depth variations of the elastic moduli pattern, closely related to variability in rock mechanical properties.

6. Conclusions

The 3D pattern of the frequency independent part of the quality factor Q_S has been determined in the Friuli Venezia Giulia Italian region and western Slovenia with attenuation tomography techniques. The k parameter was estimated on spectra corrected for the frequency dependent part of the quality factor as in Gentili and Franceschina (2011) and the 3D V_S distribution was taken from Bressan *et al*. (2012). The analysis was performed on 28 seismic stations analyzing 977 three-components seismic records corresponding to 156 earthquakes.

The analysis revealed marked lateral and depth variations of Q_S values. Three main zones have been recognized with different attenuation pattern related to the geologic-structural heterogeneity of the upper crust. The low heat flow and the variable pore pressure can also play a role in low Q_S values, but no exhaustive data on crustal fluids are available for the investigated area.

- Zone 1: the eastern part of the study area corresponding to the Kobarid region (western Slovenia) is characterized by large attenuation pattern. Low Q_S values are associated with large amount of fracturing and variable pore pressure as suggested by the highly variable V_P/V_S pattern and low heat flow characterizing the area. In detail, low Q_S pattern is associated with high shear modulus rocks of prevailing platform and dolomitic limestones, locally highly fractured, which compose the source zone of the magnitude 5.6 and 5.2 1998 and 2004 earthquakes, the most relevant events occurred in the study area in the last 30 years.
- Zone 2: the central part of the area is characterized by significant lateral variation of Q_S images, attributed to the variation of mechanical properties of the geologic units. We associate high Q_S values to Triassic and dolomitic limestones, characterized by high shear modulus and variable V_P/V_S values. Low Q_S values are associated with less competent rocks, composed by alternation of mixed carbonate-clastic limestones, dolomitic limestones and chert limestones.
- Zone 3: the Q_S images reveal a zone of low attenuation partially overlapping a zone of high attenuation. The high Q_S structure is characterized by higher shear modulus and on average lower V_P/V_S values with respect to the low Q_S zone. The variation of attenuation is attributed to the variation of the mechanical properties of the geologic units. High Q_S images are attributed to dolomitic limestones with variable density of cracks. Low Q_S images are associated with Triassic limestones and to Paleozoic sandstones and limestones.

Finally, we emphasize that the large variability in mechanical characters of the crust are related to the complex deformation pattern of the area, resulting from several tectonic phases with different orientation of the stress tensor.

Acknowledgments. We would like to thank Gianni Bressan (OGS, Udine) for his valuable discussions and suggestions. Thanks are also due to M. Živčič of the Geophysical Survey of Slovenia (Ministry of the Environment and Spatial Planning, Ljubljana) for kindly providing the waveforms of 2004 aftershocks recorded by locally temporary stations. The local seismic network is managed by the Dipartimento Centro di Ricerche Sismologiche of OGS and financially supported by the Civil Protection of the Regione Autonoma Friuli Venezia Giulia, and of the Regione Veneto, and by the Geological Survey of Provincia Autonoma di Trento. We thank the technical staff of the Department Centro di Ricerche Sismologiche (OGS) for data acquisition and processing.

REFERENCES

Abercrombie R.E.; 1998: *A summary of attenuation measurements from borehole recordings of earthquakes: the 10 Hz transition problem*. Pure Appl. Geophys., **153**, 475-487.

Adams D.A. and Abercrombie R.E.; 1998: *Seismic attenuation above 10 Hz in southern California from coda waves recorded in the Cajon Pass borehole*. J. Geophys. Res., **103**, 24257-24270.

Aki K. and Richards P.G.; 1980: *Quantitative seismology, theory and methods*, *Vol. 1*. W.H. Freeman and Company, San Francisco, CA, USA, 557 pp.

Anderson J.G. and Hough S.; 1984: *A model for the shape of Fourier amplitude spectrum of acceleration at high frequencies*. Bull. Seismol. Soc. Am., **74**, 1969-1994.

Bianco F., Del Pezzo E., Malagnini L., Di Luccio F. and Akinci A.; 2005: *Separation of depth-dependent intrinsic and scattering seismic attenuation in the northeastern sector of the Italian Peninsula*. Geophys. J. Int., **161**, 130-142.

Bressan G., De Franco R. and Gentile F.; 1992: *Seismotectonic study of the Friuli (Italy) area based on tomographic inversion and geophysical data*. Tectonophys., **207**, 383-400.

Bressan G., Bragato P.L. and Venturini C.; 2003: *Stress and strain tensors based on focal mechanisms in the seismotectonic framework of the Friuli-Venezia Giulia region (northeastern Italy)*. Bull. Seismol. Soc. Am., **93**, 1280-1297.

Bressan G., Kravanja S. and Franceschina G.; 2007: *Source parameters and stress release of seismic sequences occurred in the Friuli-Venezia Giulia region (northeastern Italy) and in western Slovenia*. Phys. Earth Planet. Inter., **160**, 192-214.

Bressan G., Gentile G.F., Perniola B. and Urban S.; 2009: *The 1998 and 2004 Bovec-Krn (Slovenia) seismic sequences: aftershock pattern, focal mechanisms and static stress changes*. Geophys. J. Int., **179**, 231-253.

Bressan G., Gentile G.F., Tondi R., De Franco R. and Urban S.; 2012: *Sequential Integrated Inversion of tomographic images and gravity data: an application to the Friuli area (north-eastern Italy)*. Boll. Geof. Teor. Appl., **53**, 191-212.

Burrato P., Poli M.E., Vannoli P., Zanferrari A., Basili R. and Galadini F.; 2008: *Sources of MW 5+ earthquakes in northeastern Italy and western Slovenia: an updated view based on geological and seismological evidence*. Tectonophys., **453**, 157-176.

Carroll D.L.; 2001: *GAFORTRAN. Genetic algorithm approach for parameter estimation*. Urbana, IL, USA, http://cuaerospace.com/carroll/ga.html

Carulli G.B., Nicolich R., Rebez A. and Slejko, D.; 1990: *Seismotectonics of the Northwest External Dinarides*. Tectonophysics, **179**, 11-25.

Castellarin A., Vai G.B. and Cantelli L.; 2006: *The Alpine evolution of the Southern Alps around the Giudicarie faults: a late Cretaceous to early Eocene transfer zone*. Tectonophys., **414**, 203-223.

Castro R.R., Pacor F., Sala A. and Petrungaro C.; 1996: *S-wave attenuation and site effects in the region of Friuli, Italy.* J. Geophys. Res., **101**, 22355-22369.

Castro R.R., Pacor F. and Petrungaro C.; 1997: *Determination of S-wave energy release of earthquakes in the region of Friuli, Italy*. Geophys. J. Int., **128**, 399-408.

Cataldi R., Mongelli F., Squarci P., Taffi L., Zito G. and Calore C.; 1995: *Geothermal ranking of Italian territory*. Geotherm., **24**, 115-129.

Console R. and Rovelli A.; 1981: *Attenuation parameters for Friuli region from strong-motion accelerogram spectra*. Bull. Seismol. Soc. Am., **71**, 1981-1991.

Cormier V.; 1982: *The effect of attenuation on seismic body waves*. Bull. Seismol. Soc. Am., **72**, S169-S200.

Dainty A.M.; 1981: *A scattering model to explain seismic Q observations in the lithosphere between 1 and 30 Hz*. Geophys. Res. Lett., **8**, 1126-1128.

De Siena L., Del Pezzo E. and Bianco F.; 2010: *Seismic attenuation imaging of Campi Flegrei: evidence of gas reservoirs, hydrothermal basins, and feeding systems*. J. Geophys. Res., **115**, B09312, doi:10.1029/2009JB006938.

Eberhart-Phillips D.; 1986: *Three-dimensional velocity structure in northern California coast ranges from inversion of local earthquake arrival times*. Bull. Seismol. Soc. Am., **76**, 1025-1052.

Eberhart-Phillips D.; 1993: *Local earthquake tomography: earthquake source regions*. In: Iyer H.M. and Hirahara K., Seismic Tomography, Theory and Practice, Chapman and Hall, New York, NY, USA, pp. 613-643.

Eberhart-Phillips D., Reyners M., Chadwick M. and Chiu J.; 2005: *Crustal heterogeneity and subduction processes: 3-D VP, VP /VS and Q in the southern North Island, New Zealand*. Geophys. J. Int., **162**, 270-288.

Evans J.R., Eberhart-Phillips D. and Thurber C.H.; 1994: *User's manual for SIMULPS12 for imaging V_P and V_P/V_S: a derivative of the "Thurber" tomographic inversion SIMUL3 for local earthquakes and explosions*. U.S. Gelogical Survey, Open File Report, 94-931, 101 pp.

Franceschina G., Kravanja S. and Bressan G.; 2006: *Source parameters and scaling relationships in the Friuli-Venezia Giulia (northeastern Italy) region*. Phys. Earth Planet. Inter., **154**, 148-167.

Galadini F., Poli M.E. and Zanferrari A.; 2005: *Seismogenic sources potentially responsible for earthquakes with M 6 in the eastern Southern Alps (Thiene–Udine sector, NE Italy)*. Geophys. J. Int., **161**, 739–762.

Gentile G.F., Bressan G., Burlini L. and De Franco R.; 2000: *Three-dimensional V_P and VP/VS models of the upper crust in the Friuli area (northeastern Italy)*. Geophys. J. Int., **141**, 457-478.

Gentili S. and Bressan G.; 2008: *The partitioning of radiated energy and the largest aftershock of seismic sequences occurred in the northeastern Italy and western Slovenia*. J. Seismol., **12**, 343-354.

Gentili S. and Franceschina G.; 2011: *High frequency attenuation of shear waves in the southeastern Alps and northern Dinarides*. Geophys. J. Int., **185**, 1393-1416.

Goldberg D.E.; 1989: *Genetic algorithms in search, optimization, and machine learning*. Addison-Wesley Publishing Company Inc., New York, NY, USA, 412 pp.

Govoni A., Bragato P.L. and Bressan G.; 1996: *Coda QC evaluation using local seismic events in the Friuli area*. In: 15° Convegno Nazionale GNGTS, Roma, Italy, pp. 389-392.

Gruppo di lavoro CPTI; 2004: *Catalogo Parametrico dei Terremoti Italiani, versione 2004 (CPTI04)*. INGV, Bologna, Italy, http://emidius.mi.ingv.it/CPTI04/.

Haberland C. and Rietbrock A.; 2001: *Attenuation tomography in the western central Andes: a detailed insight into the structure of a magmatic arc*. J. Geophys. Res., **106**, 11151-11167.

Hauksson E. and Shearer P.M.; 2006: *Attenuation models (QP and QS) in three dimensions of the southern California crust: inferred fluid saturation at seismogenic depths*. J. Geophys. Res., **111**, B05302, doi:10.1029/2005JB003947.

Hough S.E. and Anderson J.G.; 1988: *High frequency spectra observed at Anza, California: implications for Q structure*. Bull. Seismol. Soc. Am., **78**, 692-707.

Jackson I.; 2000: *Laboratory measurement of seismic wave dispersion and attenuation: recent progress*. In: Karato S., Forte A.M., Liebermann R.C., Masters G. and Stixrude L. (eds.), Earth's deep interior: mineral physics and tomography from the atomic to the global scale, Amer. Geophys. Union, Washington, DC, USA, Geophys. Monogr. Ser., **117**, 265-289.

Jackson I., Faul U.H., Fitz Gerald J.D. and Tan B.H.; 2004: *Shear wave attenuation and dispersion in melt-bearing olivine polycrystals: 1. Specimen fabrication and mechanical testing*. J. Geophys. Res., **109**, B06201, doi:10.1029/2003JB002406.

Kastelic V., Vrabec M., Cunningham D. and Gosar A.; 2008: *Neo-Alpine structural evolution and present-day tectonic activity of the eastern Southern Alps: the case of the Ravne Fault, NW Slovenia*. J. Struct. Geol., **30**, 963-975.

Lapanje A., Rman N. and Rajver D.; 2011: *Characteristics of geothermal potential, current utilization and its future (challenges) in Slovenia*. RENEXPO, Budapest, Hungary, ppt presentation.

Malagnini L., Akinci A., Herrmann R.B., Pino N.A. and Scognamiglio L.; 2002: *Characteristics of the ground motion in northeastern Italy*. Bull. Seismol. Soc. Am., **92**, 2186-2204.

Mantovani E., Albarello D., Tamburelli C. and Babbucci D.; 1996: *Evolution of the Tyrrhenian basin and surrounding regions as a result of the Africa-Eurasia convergence*. J. Geodyn., **21**, 35-72.

Michelini A. and McEvilly T.V.; 1991: *Seismological studies at Parkfield. I. simultaneous inversion for velocity structure and hypocenters using cubic b-splines parametrization*. Bull. Seismol. Soc. Am., **81**, 524-552.

Mjelde R., Raum T., Digranes P., Shimamura H., Shiobara H. and Kodaira S.; 2003: *VP/VS ratio along the Vøring Margin, NE Atlantic, derived from OBS data: implications on lithology and stress field*. Tectonophys., **369**, 175-197.

Morozov I.; 2008: *Geometrical attenuation, frequency dependence of Q, and the absorption band problem*. Geophys. J. Int., **175**, 239-252.

Morozov I.; 2010: *On the causes of frequency-dependent apparent seismological Q*. Pure Appl. Geophys., **167**, 1131-1146.

Olsen K.B., Day S.M. and Bradley C.R.; 2003: *Estimation of Q for long-period (>2 sec) waves in the Los Angeles Basin*. Bull. Seismol. Soc. Am., **932**, 627-638.

Oppenheim A.V., Schafer R.W. and Buck J.R.; 1999: *Discrete-time signal processing, 2nd edition*. Prentice-Hall, Upper Saddle River, NJ, USA, 870 pp.

Powell C., Withers M., Dunn M. and Vlahovic G.; 2006: *Anomalous VP/VS ratios in the New Madrid seismic zone: implication for seismic hazard mapping*. Seismol. Res. Lett., **77**, 107-108.

Raoof M., Herrmann R.B. and Malagnini L.; 1999: *Attenuation and excitation of three-component ground motion in southern California*. Bull. Seismol. Soc. Am., **89**, 888-902.

Rietbrock A.P.; 2001: *Wave attenuation structure in the fault area of the 1995 Kobe earthquake*. J. Geophys. Res., **106**, 4141-4154.

Schurr B., Asch G., Rietbrock A., Trumbull R.B. and Haberland C.; 2003: *Complex patterns of fluid and melt transport in the central Andean subduction zone revealed by attenuation tomography*. Earth Planet. Sci. Lett., **215**, 105-119.

Stachnik J.C., Abers G.A. and Christensen D.H.; 2004: *Seismic attenuation and mantle wedge temperatures in the Alaska subduction zone*. J. Geophys. Res., **109**, B10304, doi:10.1029/2004JB003018.

Thurber C.H.; 1993: *Local earthquake tomography: velocities and VP/VS-theory*. In: Iyer H.M. and Hirahara K., Seismic Tomography, Theory and Practice, Chapman and Hall, New York, NY, USA, pp. 563-583.

Thurber C.H. and Eberhart-Phillips D.; 1999: *Local earthquake tomography with flexible gridding*. Comput. Geosci., **25**, 809-818.

Toomey D.R. and Foulger G.R.; 1989: *Tomographic inversion of local earthquake data from the Hengill-Grensdalur Central Volcano Complex*. J. Geophys. Res., **94**, 17497-17510.

Venturini C.; 1990: *Cinematica neogenico-quaternaria del Sudalpino orientale (settore friulano)*. Volume tematico, Neogene Thrust Tectonics, Studi Geol. Camerti, Camerino, Italy, Vol. Spec., pp. 109-116.

Xie J.; 2010: *Can we improve estimates of seismological Q using a new "Geometrical Spreading" model?*. Pure Appl. Geophys., **167**, 1147-1162.

Zhou L., Zhao C., Zheng X., Chen Z. and Zheng S.; 2011: *Inferring water infiltration in the Longtan reservoir area by three-dimensional attenuation tomography*. Geophys. J. Int., **186**, 1045-1063.

Corresponding author: Stefania Gentili
Istituto Nazionale di Oceanografia e di Geofisica Sperimentale (OGS)
Sezione Centro Ricerche Sismologiche
Via Treviso 55, 33100 Udine, Italy
Tel: +39 040 2140134; fax: +39 0432 522474; e-mail: sgentili@inogs.it